OncoTargets and Therapy Dovepress

Open Access Full Text Article ORIGINAL RESEARCH

Analysis of Lymphovascular Infiltration and Tumor-Associated Macrophages in Cervical Cancer Immunoescape

Liming Guan[1], Xuexiang Xu[1], Junhao Xu[2], Gang Xu[3], Yunzhu Zhang[4], Haitao Xia[1]

[1]Department of Obstetrics and Gynecology, Zhabei Centrial Hospital, Jing'an District, Shanghai, 200070, People's Republic of China; [2]Clinical Medicine2020, Capital University of Medical Sciences, Fengtai District, Beijing, 100069, People's Republic of China; [3]Department of Radiation Oncology, Cancer Hospital & Institute, Haidian District, Beijing, 100142, People's Republic of China; [4]Department of Obstetrics and Gynecology, Pudong New Area People's Hospital, Shanghai, 201299, People's Republic of China

Correspondence: Liming Guan, Email guanliming1@126.com

Background: Exact detection of lymphovascular infiltration (LVI) status can guide accurate surgical operation scope in cervical cancer, but LVI reduces the overall survival (OS) of patients and is not easily detected by hematoxylin–eosin (H&E) staining. The role of tumor-associated macrophages (TAMs) in this process is not well defined.

Methods: Early-stage cervical cancer patients received carbon nanoparticles for sentinel lymph-node mapping, laparotomy pelvic lymph-node dissection, and radical hysterectomy. The excised specimens were analyzed using ultrastaging, double immunohistochemical (IHC) staining, flow cytometry, and Western blot analysis. Single-cell data from the Gene Expression Omnibus for cervical cancer were obtained and analyzed.

Results: The integration of carbon nanoparticle mapping, ultrastaging, and double IHC staining enhanced the detection of tumor LVI over H&E staining (41.8% [41/98] vs. 20.4% [20/98], P=0.046). When the number of vascular invasion foci was greater than two, there was a negative correlation with OS (P<0.05). More M2 TAMs emerged surrounding the tumor vasculature labeled by double IHC staining, accompanied by a higher M2:M1 ratio detected with flow cytometry (P<0.05). M2 TAM numbers were positively correlation with the degree of tumor LVI (P=0.0024), combined with higher protein expression of MMP2, SPARC, and GNLY in the tumor LVI-positive group on Western blot analysis, and the OS of the patients decreased accordingly. Single-cell data showed that the M1:M2 ratio decreased significantly, accompanied by higher M2 TAM-related gene expression. Immunosurveillance and anti-immun oescape scores for M1 were obviously higher than for M2 TAMs. GO and KEGG analysis showed M2 TAM activity increased from precancerous lesions to cervical cancer.

Conclusion: Combining different methods may accurately determine tumor LVI status, guide exact surgical operation scope, and improve cervical cancer patient outcomes. M2 TAM activity increased in cervical cancer, forming an immunosuppressive environment, TAM-related genes could be good markers in determining cervical cancer LVI and serve as potential targets for immunotherapy.

Keywords: cervical cancer, double immunohistochemical staining, lymphovascular infiltration, LVI, tumor-associated macrophages, TAMs, single-cell data analysis

Introduction

Cervical cancer is the most prevalent malignancy among women in developing countries. Cervical cancer metastasis accounts for 90% of patient deaths. Even if no lymph-node metastasis is detected by hematoxylin–eosin (H&E) staining, 15% of patients still experience recurrence and metastasis, among which pelvic lymph-node recurrence accounts for about 67%, indicating the existence of micrometastases that cannot be detected by traditional pathological detection. Once regional lymph-node metastasis is present, the 5-year survival rate is only 30%-60%.[1]

National Comprehensive Cancer Network guidelines recommend accurate medical treatment and sentinel lymph node (SLN) biopsy instead of pelvic lymph-node dissection to avoid lymphocysts and immune-system damage for early-stage

Received: 27 June 2024
Accepted: 29 October 2024
Published: 20 November 2024

cervical cancer.[2] However, it has been reported that laparotomy enhanced the rate of disease-free survival and overall survival (OS) for cervical patients over those that received laparoscopic operations. As such, only laparotomy is currently recommended for cervical cancer patients.[3] Both surgical procedures face the same problem: how to find tumor lymphovascular micrometastasis in time.

"Vasculature emboli" refers to tumor cells infiltrating lymphatic or vascular lumina, including lymphatic and vascular emboli. As it is difficult to distinguish small veins, small arteries, and small lymphatic vessels in H&E staining using light microscopy, in this paper we refer to "vasculature infiltration" or "lymphovascular infiltration" (LVI), except where labeled by specific immunohistochemical (IHC) markers.[4] Tumor LVI is one of the high-risk factors for cervical cancer. The formation of vasculature tumor emboli indicates that tumor cells have infiltrated the vascular system, which often indicates the degree of malignancy of the tumor and is a poor prognostic indicator. It is associated with distant metastasis and renders the patient incurable.[5,6] Lymphatic metastasis is the main metastasis pathway of cervical cancer. Accurate determination of the presence or absence of tumor metastasis and the extent of metastasis can provide reference for prognoses of cervical cancer patients and individualized treatment-plan formulation.[6]

It has been found that perivascular tumor-associated macrophage (TAM) aggregation increases tumor proliferation and metastasis, while tissue pathological detection cannot provide accurate information on individual cells in a complex tumor environment. Single-cell sequencing analysis can visualize individual cell types in cervical cancer tissue, but there are few reports on the combination of clinicopathological examination with TAM single-cell analysis.In this study, cervical cancer lymphovascular micrometastasis states were preliminarily screened by carbon nanoparticle (CNP) mapping, followed by H&E and double IHC staining, The role of TAMs in the tumor microenvironment was analyzed by IHC staining, flow cytometry, Western blot, and single-cell data.

Methods

Patient Characteristics and Enrollment

This prospective study was conducted on patients with cervical cancer. From 2019 January to January 2023, 110 women with cervical cancer stage within IIB according to the International Federation of Gynecology and Obstetrics (FIGO) 2018 standard were enrolled at Zhabei Central Hospital, among whom 98 patients were included in this study. A total of 98 patients gave informed consent and were fully evaluated for eligibility to participate in the study.

The study was approved by the ethics committee of Zhabei Centrial Hospital (ZBLL2022102402001) and designed in line with the Declaration of Helsinki in terms of human rights. The patients were informed of the risks and benefits of participating in the study, signed written agreements. These patients come from Shanghai, the Yangtze River Delta, and from all over China. The number of subjects required was calculated with PASS software.

Inclusion criteria were histopathologically confirmed cervical cancer within FIGO (2018) ≤IIB, tumor diameter ≤4 cm, and physically fit for extensive surgical procedures. Exclusion criteria were advanced cervical cancer (FIGO stages III–IV) with obvious retroperitoneal lymph-node metastasis or distant metastasis, allergy to CNPs, history of cervical or pelvic surgeries causing severe adhesions, and preoperative radiotherapy. Patients' ages ranged from 26 to 74 years, with an average age of 55.3 years. Twelve cervical cancer patients and those with other malignant tumors or incomplete clinical data were excluded.

Inclusion and exclusion criteria were met by 89.1% (98/110) patients, with 10.09% (12/110) exiting the study without treatment: two rejected treatment at the hospital, six had advanced cervical cancer (FIGO stages III–IV), and four had had previous major operations in the pelvis, had recurrent cervical cancer, or had a history of pelvic radiotherapy. These 98 patients received CNP mapping + laparotomy pelvic lymph-node dissection + radical hysterectomy within 6 months. After the surgery, patients were followed up from January 2019 to January 2023 to track OS and recurrence-free survival (RFS).

SLN Biopsy

The patients received general anesthesia under lithotomy position. About 1 mL of CNPs was administered at 3 and 9 o'clock around the cervical tumor lesion. The depth of needle injection was 0.2±0.6 cm from the epidermis, and

administration was finished in 3–4 minutes. A tiny piece of gauze was pressed onto the injection site to prevent the reagent from leaking. Black-stained lymphatic vessels were determined during the laparotomy. The first appearance of black-stained lymph nodes within 10 minutes or enlarged palpable nodes detected were defined as SLN-positive, while the lymph nodes that stained black after 10 minutes were defined as non-SLNs. When black-dyed or enlarged palpable nodes could not be determined during the operation, we regarded CNP lymph-node mapping to be negative.

The number and location of SLNs and non-SLNs were recorded. The SLN specimens were resected for frozen pathology alone. Next, all patients underwent laparotomy radical hysterectomy and pelvic lymph-node dissection (and/or para-aortic lymph-node sampling). The negative specimens on CNP mapping were detected by ultrastaging section and double IHC staining. H&E staining and double IHC staining were compared for detection of LVI using two different detection methods. Ratios between groups were assigned one by one for the CNP mapping–negative patients. The CONSORT flow diagram for the study is displayed in Figure 1.

Pathological Examination

In sum, 98 cases of surgically resected lymph nodes and cervical tumor tissue were embedded in paraffin. The samples were divided perpendicularly to their long axis into 5 μm slides, received routine H&E and single and double IHC staining, respectively.

Quality Standards for H&E Staining

Sections of 4–6 μm thickness were stained dark red and blue, seal frames were clean and transparent, and thickness was uniform without wrinkles or knife marks.

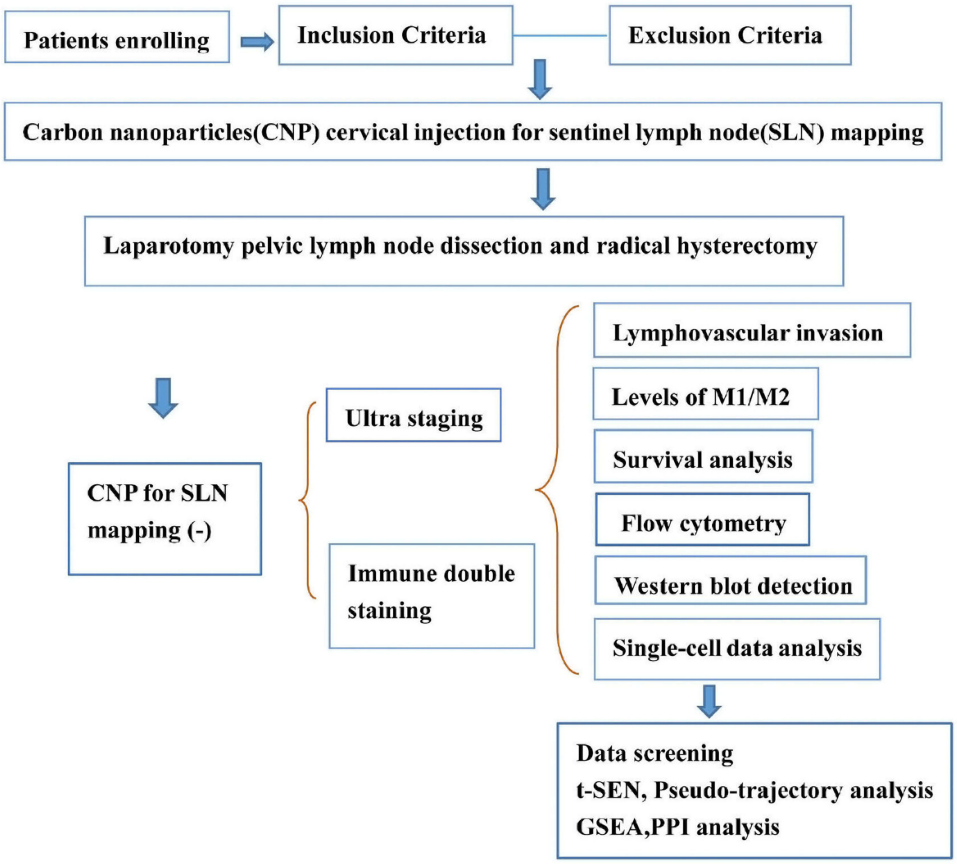

Figure 1 CONSORT flow diagram for the study.

IHC Staining

Sections 5 μm thick were cut from formalin-fixed, paraffin-embedded tissue. Sections were dewaxed with dimethylbenzene for 10 min. Endogenous peroxidase activity was blocked with methanol containing 0.3% hydrogen peroxide for half an hour, followed by rehydration in a series of graded alcohol for 40 min. Antigen retrieval was carried out via citric acid in an autoclave at 2 atmospheres of pressure and 121°C for 10 min. Slides were blocked with bovine serum.

Next, sections were labeled with the primary antibodies D2-40, CD31, CKpan, CD68 (PGM1 or KP1), CD163, and CD206 at 5°C for 12h. Anti-mouse labeled with streptavidin–biotin peroxidase and anti-rabbit labeled with the EnVision-HRP polymer system were used as the secondary antibodies. A positive reaction for D2-40 (or CD31) was detected as brown coloration with diaminobenzidine (DAB) as substrate, and another positive reaction for CKpan (CD68, CD163 or CD206) was detected as ligh-red coloration with Vulcan fast red as substrate. Finally, hematoxylin counterstained the sections.

Double-Antibody IHC Staining

The slices were stained with D2-40/CKpan for tumor lymphatic invasion or CD31/CKpan for vascular invasion; both labeled brown/red. The lymphangion/TAM double-IHC-staining protocols were similar to the aforementioned vasculature/tumor double IHC staining. The slices were stained with D2-40/CD68 (PGM1 or KP1) for lymphangion/M1 macrophages or D2-40/CD163 (or CD206) for lymphangion/M2 macrophages, both labeled brown/red. CD68 (PGM1 or KP1) was the M1 macrophage marker, and CD163 and CD206 were M2 macrophage markers. $CD68^{+}$, $CD163^{-}$, and $CD206^{-}$ cells were regarded as M1 TAMs. $CD163^{+}$ and $CD206^{+}$ cells were regarded as M2 TAMs. When $CKpan^{+}$ cervical cancer cells were detected within the intraluminal region of $D2\text{-}40^{+}$ lymphatic vessels, this was regarded as lymphatic invasion.[7]

Pathological imaging was quantified with ImageJ. Regions of interest (ROIs), TAMs, and tumor lymphovascular foci structures were outlined by hand-drawing or thresholding. The formula for the fluorescence intensity of an ROI was: mean fluorescence intensity = sum of fluorescence intensity in the region (IntDen)/area. We defined tumor LVI focus intensity and TAM density as cervical cancer LVI cell numbers and TAM cell numbers, respectively. Positive cervical cancer LVI cells and TAMs within the lymphovascular lumen within five fields of cervical cancer tissue under 40× microscopic power were counted, then the average calculated.

Automated Blood-Cell Analyzer and Flow Cytometry

Leukocyte classification and M1 and M2 TAMs were detected by both an automated blood cell analyzer and flow cytometry. M2 and M1 cell numbers and M2:M1 TAM ratio were calculated by monocytes count × IHC ratio and flow cytometry by M1 and M2 TAM count. Four-color flow-cytometry analysis was performed using a BD FACSCalibur. Peripheral venous blood samples were collected from patients and transferred into EDTA-coated tubes. Blood samples (100 μL) were labeled with different monoclonal antibodies. Cell-surface monocyte phenotypic analysis was performed after staining with human anti-CD14 and anti-CD16. Phenotypic monocytes were labeled with antibodies of CD68, CD86, and CD206. Cells were incubated for 30 min at room temperature with the optimal dilution of each antibody according to the manufacturer's instructions. The frequencies of the different subpopulations were calculated using FlowJo_version 10 (BD Biosciences). All reagents and their sources used are listed in Table 1.

Western Blot Analysis

Based on our double-IHC-staining results, the patients were divided into cervical cancer LVI- positive and -negative groups. Cervical cancer tissue were taken from these two groups for Western blot analysis. Cervical cancer tissue was lysed with RIPA lysis buffer. The lysed cells were separated by centrifugation at 12,000 revolutions for 5 minutes. The supernatant was collected. Electrophoresis was performed on a sodium dodecyl sulfate polyacrylamide gel. The electrophoresed products were transferred to nitrocellulose membranes. The primary antibodies used in this study were MMP2 (rabbit anti-human 1:200, Abcam), SPARC (rabbit anti-human 1:200, Santa Cruz), and GNLY (mouse anti-human 1:100, Invitrogen). The secondary antibodies were conjugated with horseradish peroxidase, and protein

Table 1 Primary antibodies used in this study

IHC antibody	Species, isotype	Source	Dilution
D2-40	Mouse, $IgG_1\kappa$	Dako, Carpinteria, CA, USA	×50
CD31	Rabbit, IgG	Yubo Biotechnology	×100
CKpan	Rabbit, IgG	Shanghai QiMing Biotechnology	×100
CD68 (PGM1)	Mouse, $IgG_1\kappa$	Yubo Biotechnology	×50
CD68 (KP1)	Mouse, $IgG_3\kappa$	Yubo Biotechnology	×50
CD163	Mouse, IgG_1	Abcam, Cambridge, UK	×100
CD206	Mouse, $IgG_1\kappa$	Abcam, Cambridge, UK	×200
Flow-cytometry antibody	**Fluorochrome**	**Source**	
CD14	Allophycocyanin	Yubo Biotechnology	
CD16	Fluorescein isothiocyanate	Yubo Biotechnology	
CD68	Fluorescein isothiocyanate	Yubo Biotechnology	
CD86	Phycoerythrin–cyanine 7	Yubo Biotechnology	
CD206	Phycoerythrin	Yubo Biotechnology	

production was detected by Western blot detection reagents (Thermo Fisher Scientific). β-actin was used as an internal reference.

Determination Standards

Based on the location, degree, and number of invading cancer cells, the patients were further divided into three groups: intramural vascular invasion including mucous membrane, submucosa, and musculi propria; extramural vascular invasion beyond the musculi propria; and both intramural and extramural vascular invasion.

Based on the number of paraffin sections and lesions positive for vascular invasion, the patients were divided into three groups: local invasion, moderate invasion, and extensive invasion.Only one tumor focus of vascular invasion detected was defined as local invasion. More than one tumor focus of vascular invasion detected, but limited to one paraffin section, was defined as moderate invasion. More than one tumor focus of vascular invasion detected and tumor foci distributed in different paraffin sections was defined as extensive invasion. The cutoff values were calculated for the number of vascular tumor foci and the number of tumor cells within tumor foci. The sensitivity and specificity of double IHC staining were evaluated.

The macrometastases (diameter >2 mm) of lymph nodes and tumor tissue were sectioned. Macrometastases were defined as a single focus of metastatic tumor tissue per node measuring more than 2 mm, micrometastases as a focus of metastatic tumor tissue ranging from 0.2 mm to no more than 2 mm, and submicrometastases as metastases measuring no more than 0.2 mm (including the presence of a single noncohesive tumor cell). Lymph nodes were considered positive when they included macrometastases, micrometastases, or submicrometastases. Similarly, when tumor metastases were within lymphatic or vascular lumina, they were defined as LVI.[5]

Cervical Cancer Single-Cell Data Collection and Analysis

Microarray datasets for the GSE208653 datasets were obtained from the Gene Expression Omnibus (GEO) database, which included three cervical cancer samples (https://www.ncbi.nlm.nih.gov/geo/query/acc.cgi?acc=GSE208653). These samples contained the normal cervical tissue, precancerous and cervical cancer tissue, and metastatic lymph nodes. We performed single-cell analysis using these data.

Cell-Quality Screening and Cell-Type Determination

Cell type and quality was evaluated with the Seurat package. When unique molecular identifiers (UMIs) were fewer than 200 or the mitochondrion's original UMI number was over 10%, the data were not included. The top 15 primary components and first 2000 key genes were included in this study. The data were normalized with the "scale data" function. The cell clusters were determined by the "find clusters function" and analyzed with the Louvain clustering algorithm-embedded method. Next, the data were visualized with the "t-distributed stochastic neighbor embedding" (t-SNE) function, and cell-type markers were defined.

Pseudotrajectory Construction

The data were reduced in dimension and cell types were arranged. M1 and M2 macrophage subgroups were visualized for pseudotrajectories with Monocle 2 packages. Different genes were determined with differential gene test functions in an unsupervised manner.

Differentially Expressed Genes (DEGs) for Gene Set Enrichment Analysis (GSEA)

The "find all markers" function was used to standardize cluster marker expression. Differential pathways were enriched and analyzed by Kyoto Encyclopedia of Genes and Genomes (KEGG) and Gene Ontology (GO) function in the ClusterProfiler series package. The ligand and receptor connections for TAMs that determine cervical cancer metastasis were analyzed with the "protein–protein interaction" function at https://string-db.org/.

Statistical Methods

GraphPad 6.0 software was used for statistical analysis. H&E staining and double IHC staining, two efficient approaches for determining tumor vascular invasion, were evaluated by κ consistency test (consistency test) and Wilcoxon signed-rank test (Mann–Whitney *U* test). Correlations were analyzed by the χ^2 test and Fisher's exact probability method. Single-factor survival rates were determined by the Kaplan–Meier method, and differences between groups were compared with the log-rank test. $P<0.05$ was considered statistically significant.

Results

Preliminary CNP Screening of SLN Invasion for Cervical Cancer

We performed a screening for the distribution of pelvic lymph nodes with CNPs preliminarily. Among the 98 patients, 96 had more than one SLN. The detection rate was 96.9% (96/98). A total of 356 SLNs were found, with a mean of 3.4 SLNs for each side. Lymph nodes were determined in the obturator (43.25%), internal lilac (15.46%), external lilac (23.54%), parametrial (5.32%), and common iliac (5.45%) regions. The sensitivity of the SLN detection was 98.0% (96/98), the accuracy rate was 96.1% (94/98), the negative prediction rate was 100%, and the false-negative rate was 0.

Tracer CNPs were intracervically injected in uterine cervical cancer (see Figure 2A, arrow). SLNs labeled with CNPs stained black (Figure 2B, arrow). Tumor occult metastases labeled by CNP within SLNs can be seen in Figure 2C (arrow). Normal cervical lymph nodes were used as a negative control (Figure 2D). Cervical tissue was stained black by CNPs (Figure 2E, arrow). The CNPs served as a preliminary tracer for SLNs in cervical cancer to detect LVI.

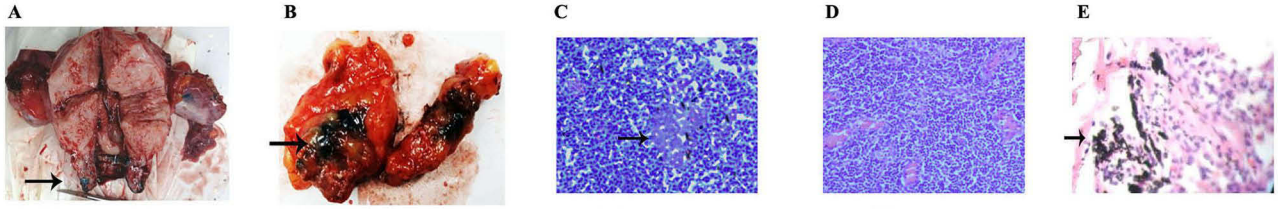

Figure 2 Carbon nanoparticles (CNPs) for sentinel lymph node (SLN) mapping. (**A**) Intracervical injection of CNPs (arrow). (**B**) SLNs stained black by CNPs (arrow). (**C**) Tumor metastases labeled by CNPs within SLNs (arrow). (**D**) Normal cervical lymph nodes as negative control. (**E**) Cervical tissue stained black by CNPs (arrow).

Double IHC Staining Enhanced Cervical Cancer LVI Detection

Next, we carried out H&E and IHC detection for resected cervical cancer samples. Tumor foci exhibiting an elongated and fragmented appearance may be difficult to determine, and a single tumor cell may appear to be similar to a normal cervical histiocytoid. It is not easy to distinguish artificial fissures from tumor LVI under H&E staining.

In 98 cases of specimens for cervical cancer, double IHC staining was positive for vasculature invasion in 51 cases (52.04%) and negative in 47 cases (47.96%). Three of the positive cases were confirmed by IHC staining as retraction fissure rather than vasculature invasion. H&E staining was confirmed by double IHC staining. Vasculature invasion detected by double-stained sections can also rule out possible false positives and some tiny LVIs that are difficult to confirm under H&E sections.

Neither H&E staining nor D2-40 IHC staining confirmed lymphovascular lumen content as tumor tissue (Figure 3Ai and Aii, arrow). Neither H&E staining nor CKpan IHC staining confirmed tumor tissue in lymphovascular lumina (Figure 3Bi and Bii, arrow). CD31/CKpan double staining confirmed cervical cancer vascular invasion (Figure 3Ci, arrow). D2-40/CKpan double staining confirmed cervical cancer lymphatic metastasis (Figure 3Cii, arrow).

Subsequently, we evaluated IHC double-staining detection efficiency on tumor LVI foci with receiver operating characteristic (ROC) curves. When the cutoff for cervical cancer LVI foci was two, the area under the ROC curve was 0.8709 (sensitivity 79.59%, specificity 83.67%, $P<0.0001$; Figure 3Di and Table S1). When the cutoff for cervical cancer cell numbers within LVI foci was 5.3, the area under the ROC curve was 0.9363 ($P<0.0001$, Figure 3Dii and Table S2). Therefore, IHC double staining demonstrated higher detection efficiency for tumor LVI foci.

In addition to improving the detection rate, double IHC staining also detected more lesions of LVI ($P<0.05$, Wilcoxon symbolic rank test). Consistency analysis showed H&E staining and double IHC staining for evaluation of LVI had medium consistency ($\kappa=0.4585$, $P<0.05$; Wilcoxon symbolic rank test, Table 2). The average rate of cancer foci/paraffin block for 26 patients with LVI was determined by both H&E staining and double IHC staining. The average rate of cancer foci/paraffin block confirmed by double IHC staining was significantly higher than that of H&E staining (3.82 vs. 1.79, 95% CI 1–2 vs. 3–4.6, $P<0.001$; Wilcoxon signed-rank test). If double IHC staining were used as the gold standard for the assessment of LVI, the sensitivity and specificity of H&E staining were 50.98% and 60.74%, respectively. To sum up, we integrated methods of CNP mapping, ultrastaging, and double IHC staining, and these methods enhanced the ratio of determination of tumor LVI over H&E staining.

Cervical Cancer LVI Status Closely Related to Prognosis of Patients

We followed up on the patients and analyzed the relationship between tumor LVI and prognosis. D2-40/CD31-CKpan IHC staining showed positive vasculature invasion in 51 cases (52.04%), and the patients were further divided into subgroups according to the location and degree of vasculature invasions, as well as the number of tumor cells in lymphovascular invasive foci. The location and degree of vasculature invasion correlation with the OS of patients were analyzed. The mean OS of the vasculature invasion–positive group was obviously lower than the vasculature invasion–negative group. There was a significant difference between the two groups (68.5±7.4 vs. 48.2±6.5 months, $P<0.05$; Kaplan–Meier curve method and log-rank test, Figure 4A and Table S3).

Among the 51 tumor LVI–positive patients, there were 21 cases of intravascular invasion (41.18%), 16 of extravascular invasion (31.37%), and 14 of both intravascular invasions and extravascular invasion (27.45%). The OS for patients with different vasculature invasive locations was compared. The longest OS was for intravascular tumor invasion, followed by extravascular tumor invasion group, and the shortest OS was for both tumor intravascular invasion and extravascular invasion (51.3±7.4 vs. 38.7±6.2 vs. 15.4±5.3 months, $P<0.05$; Kaplan–Meier curve method and log-rank test, Figure 4B and Table S4).

There were 23 cases of local invasion (45.10%, n=51), 19 cases of moderate invasion (37.25%), and nine cases of extensive invasion (17.65%). The OS for patients with different degrees of vasculature invasion was compared. The longest OS was for local tumor invasion group, followed by moderate tumor invasion, and the shortest OS was for extensive tumor invasion (54.6±7 vs. 32.5±5.4 vs. 13.8±5.5 months, $P<0.05$; Kaplan–Meier curve method and log-rank test, Figure 4C and Table S5).

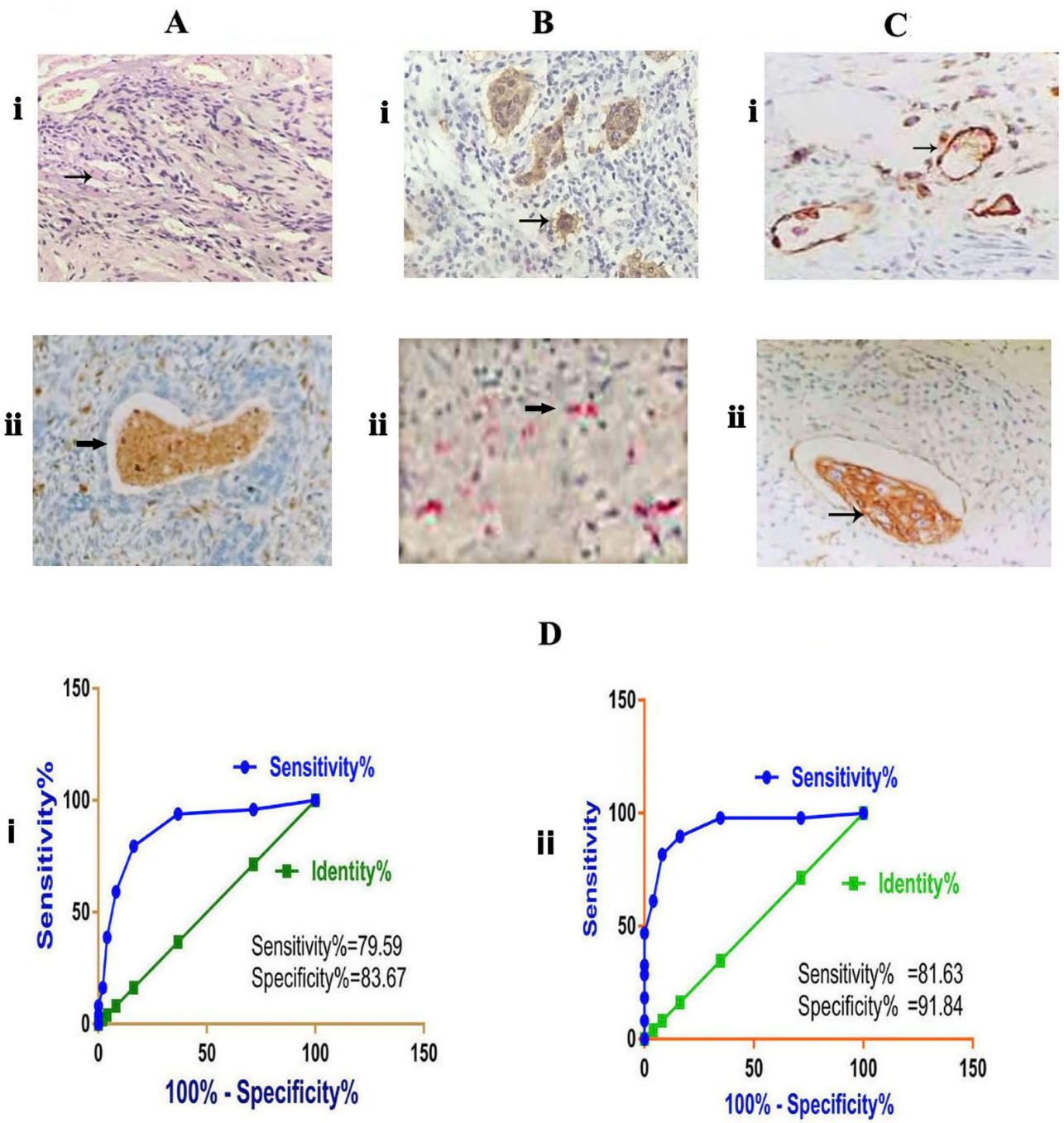

Figure 3 Double IHC staining enhanced cervical cancer LVI detection. (**Ai**) H&E staining and (**Aii**) D2-40 IHC staining could not confirm lymphovascular lumen content as tumor tissue (arrow). (**Bi**) H&E staining and (**Bii**) Ckpan IHC staining could not confirm tumor tissue with lymphovascular lumen (arrow). (**Ci**) CD31/CKpan double staining confirmed cervical cancer vascular invasion (arrow). (**Cii**) D2-40/CKpan double staining confirmed cervical cancer lymphatic metastasis (arrow). (**Di**) ROC curve of detection efficiency for number of tumor LVIs. (**Dii**) ROC curve of detection efficiency for number of tumor cells/tumor focus.

There were 39 patients with two or fewer tumor LVI foci (76.47% and 12 (23.53%, n=51) with more than two. Among these 39 patients, <5.3 tumor cells/tumor focus were detected in 19 (48.7%) and >5.3/tumor focus determined in 20 patients (51.3%). The OS for patients with different numbers of invading tumor cells was compared. There was longer OS in the group with <5.3 tumor cells/tumor focus than the group with >5.3 tumor cells/tumor focus. There was a significant difference between the groups (41.3±7.5 vs. 32.5±6.6 months, P<0.05; Kaplan–Meier curve method and log-rank test, Figure 4D and Table S6). Therefore,

Table 2 Contrasting of D2-40/CD31-CKpan double and H&E staining in determining vasculature invasion

		D2-40/CD31-CKpan		Sum	κ	*P*
		Positive	**Negative**			
H&E label	Positive	26	2	28	0.4585	<0.001
	Negative	25	45	70		
Sum		51	47	98		

LVI in cervical cancer is closely related to the OS of patients, and the OS depends on its location, degree, and number of tumor foci.

In this study, potential confounding factors were controlled for during the analysis with instrumental variable analysis (IVA). Additional statistical tests were used to confirm Kaplan–Meier and Cox regression analysis results. To avoid type I errors, we ensured a sufficient quantity of samples and set significance to $P<0.05$, even 0.001, for the null hypothesis to be rejected. To avoid type II errors, we performed hypothesis testing using the Neyman–Pearson approach. In these ways, the accuracy and reliability of statistical inference were improved.

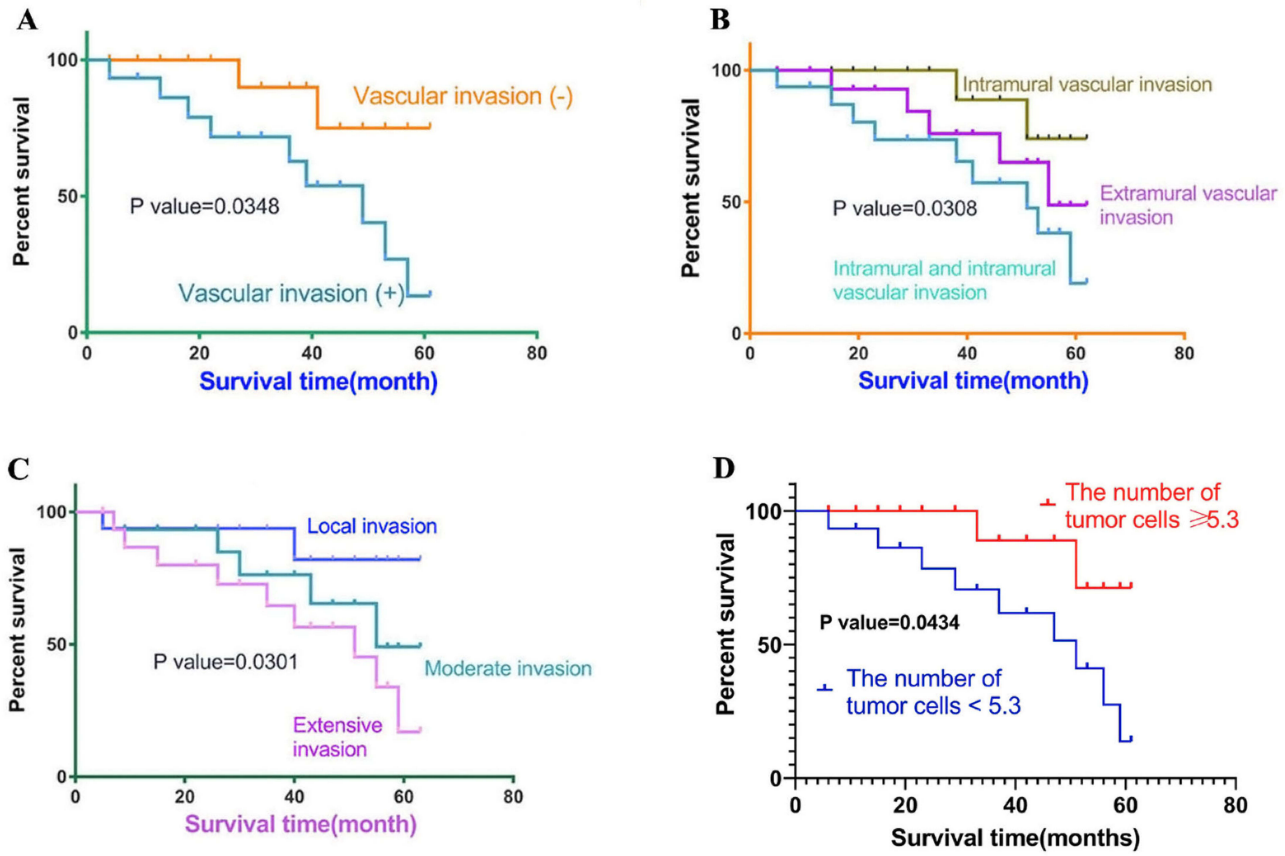

Figure 4 Cervical cancer lymphovascular infiltration (LVI) decreased overall survival (OS) of patients. (**A**) Correlation of tumor LVI with OS. (**B**) Comparison of OS and different tumor LVI locations. (**C**) Comparison of OS and different degrees of LVI. (**D**) Comparison of OS and number of tumor cells/tumor focus.

Table 3 Clinicopathological status of patients and cervical cancer LVI (n=98)

	Lymphovascular Invasion		Significance	M1/M2		Significance
	Positive n=51	Negative n=47		High n=40	Low n=48	
Age, year						
<50	39 (54.2)	33 (45.8)	χ^2=0.04957	30 (44.8)	37 (55.2)	χ^2=0.05212
≥50	15 (51.2)	14 (48.8)	*P*=0.8238	10 (47.6)	11 (52.4)	*P*=0.8194
Histotype						
Squamous	41 (50.3)	39 (49.7)	χ^2=0.1091	25 (48.1)	27 (51.9)	χ^2=0.3626
Adenocarcinoma	10 (55.6)	8 (44.4)	*P*=0.7411	15 (41.7)	21 (58.3)	*P*=0.5527
Tumor grade						
G1/G2	35 (51.5)	33 (48.5)	χ^2=0.02894	25 (40.3)	37 (59.7)	χ^2=2.229
G3	16 (53.3)	14 (46.7)	*P*=0.8649	15 (57.8)	11 (42.3)	*P*=0.1354
FIGO stage						
IB	15 (39.5)	23 (60.5)		20 (46.5)	23 (53.5)	
IIA	16 (51.6)	15 (48.4)	χ^2=5.678	12 (46.2)	14 (53.9)	χ^2=0.1105
IIB	20 (69)	9 (31)	*P*=0.0172	8 (42.1)	11 (57.9)	*P*=0.9463
TAMs, n				12 (0–43)	15 (0–47)	*P*=0.8492
M1, n				7 (1–26)	2 (1–12)	*P*<0.05
M2, n				2 (0–23)	9 (1–36)	*P*<0.001
Monocyte count/μL				490 (220–1140)	520 (19–780)	*P*=0.5325

Clinicopathological Status of Patients Promoting Cervical Cancer LVI

Then, we analyzed the factors affecting the LVI of cervical cancer. Based on clinicopathological screening, the LVI-positive group showed no significant correlation with age or histotype ($P>0.05$, χ^2 test), but there were correlations with FIGO stage, tumor grade, and levels of M1/M2 TAMs ($P<0.05$, χ^2 test; Table 3). In contrast to low-M1:M2 TAM-ratio patients, patients with high M1/M2 TAMs displayed a 5-year longer disease-free period (71.4% vs. 46.4%, $P<0.05$, χ^2 test) and 5-year longer OS (73.9% vs. 48.2%, $P<0.05$, χ^2 test).

M2 TAM Polarity Facilitated Cervical Cancer LVI

We detected M1 and M2 TAM distribution in cervical cancer tissue by double IHC staining. It showed lymph vessels (D2-40, brown) surrounded tumor cells and M1 TAMs (red, CD68, PGM1) in cervical cancer tissue (Figure 5Ai). The count of positive M1 TAMs in cervical cancer was obviously less than that of normal cervical tissue, and there were significant differences between the two groups (23.17±2.857 vs. 32.67±2.83, $P<0.05$, unpaired *t* test; Figure 5Aii and Table S7). All the same, lymph vessels and M1 TAMs were double-stained by D2-40 and CD68 (KP1; Figure 5Bi). The count of positive M1 TAMs within lymph vessels of cervical cancer was obviously less than that of normal cervical tissue, with obvious differences between the two groups (22.33±2.525 vs. 34.83±3.745, $P<0.05$, unpaired *t* test; Figure 5Bii and Table S8). Lymph vessels and M2 TAMs were double-stained by D2-40 and CD163 (Figure 5Ci). The count of $CD163^+$ M2 TAMs within lymph vessels of cervical cancer and normal cervical tissue were compared, and there were obvious differences between the two groups (2.33±2.66 vs. 17.83±2.257, $P<0.05$, unpaired *t* test; Figure 5Cii and Table S9). Lymph vessels and M2 TAMs were double-stained with D2-40 and CD206 (Figure 5Di and Ei. Counts of M2 TAMs within lymph vessels of cervical cancer and normal cervical tissue were compared, and there were obvious differences between the two groups (24.83±2.561 vs. 12.00±1.789, $P<0.05$, unpaired *t* test; Figure 5Dii and Table S10).

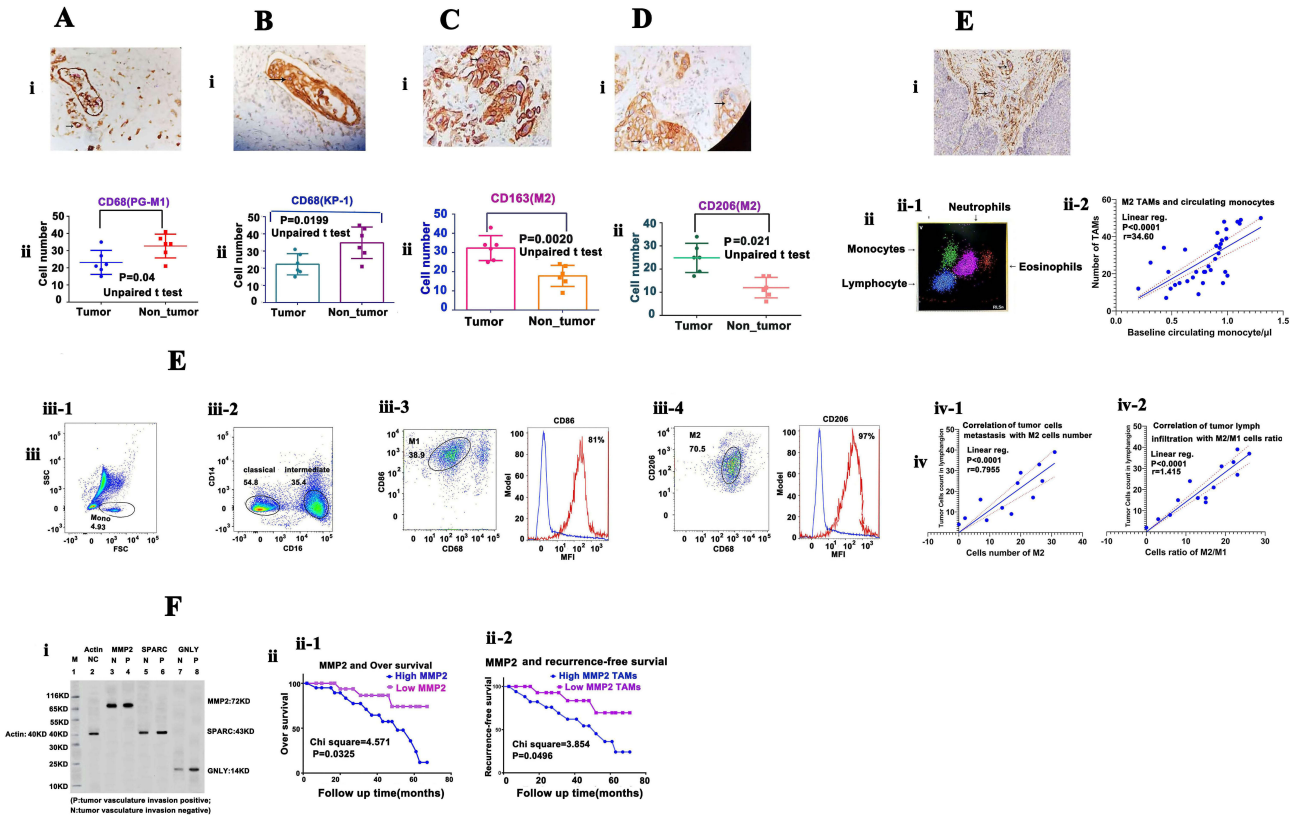

Figure 5 Tumor lymphatic infiltration and tumor-associated macrophages (TAMs). (**Ai**) Lymph vessels (D2-40, brown) surrounded tumor cells and M1 TAMs (red, CD68, PGM1) in cervical cancer. (**Aii**) The count of positive M1 TAMs in cervical cancer was obviously lower than that in normal cervical tissue. (**Bi**) Lymph vessels (D2-40, brown) surrounded cervical cancer cells and M1 TAMs (red, CD68, KP1). (**Bii**) The count of positive M1 TAMs in cervical cancer was obviously lower than that in normal cervical tissue. (**Ci**) Lymph vessels (D2-40, brown) surrounded cervical cancer cells and M2 TAMs (red, CD163). (**Cii**) The count of positive M2 TAMs in cervical cancer was obviously higher than in normal cervical tissue. (**Di** and **Ei**) Lymph vessels (D2-40, brown) surrounded tumor cells and M2 TAMs (red, CD206) in cervical cancer tissue. (**Dii**) The count of positive M2 TAMs in cervical cancer was obviously higher than that in normal cervical tissue. (**Eii-1**) Automatic blood cell analysis of leukocyte classification. (**Eii-2**) Ratio of M2:M1 TAMs calculated according to double IHC staining. Count of M2 TAMs based on number of monocytes by linear regression analysis. (**Eiii-1, iii-2, iii-3,** and **iii-4**) Flow cytometry: (**Eiii-1**) scatterplot of leukocyte classification; (**Eiii-2**) scatterplot of monocytes of classical (CD14) and intermediate (CD16) subtypes; (**Eiii-3**) scatterplot and intensity map of M1 TAMs (CD86); (**Eiii-4**) scatterplot and intensity map of M2 TAMs (CD206). (**Eiv-1**) Correlation of tumor metastases with number of M2 TAMs in cervical cancer. (**Eiv-2**) Correlation of tumor metastases with M2:M1 TAM ratio, indicating cervical cancer lymphatic infiltration accompanied by increase in M2 TAMs. (**Fi**) Protein expression for MMP2, SPARC, and GNLY in cervical cancer LVI-positive group was obviously higher than that of negative group (Western blot analysis). (**Fii-1**) OS of patients was obviously higher in lower MMP2-expression group than in higher MMP2-expression group. (**Fii-2**) Relapse-free survival (RFS) was obviously higher in lower MMP2-expression group than higher MMP2-expression group.

We calculated the ratio of M2:M1 TAMs based on double-IHC-staining results. There were obviously more M2 TAMs in the tumor lymphatic infiltration-positive group than the lymphatic infiltration-negative group (unpaired *t* test, $P<0.05$). Subsequently, we detected baseline circulating monocytes (number/μL) using the automatic blood cell analyzer. The count of M2 TAMs based on the monocytes was analyzed by linear regression analysis (Figure 5Eii-1; Figure 5Eii-2 and Table S11). Then, we detected leukocyte types with flow cytometry. The results are presented in Figure 5Eiii-1. Monocytes of classical (CD14) and intermediate (CD16) subtypes detected by flow cytometry are presented in Figure 5Eiii-2. M1 TAMs (CD86) are presented in Figure 5Eiii-3, and M2 TAMs (CD206) are presented in Figure 5Eiii-4.

The correlation of M2 TAM numbers and the extent of tumor lymphatic infiltration in cervical cancer was analyzed ($P=0.0024$, $r=0.9771$, linear regression; Figure 5Eiv-1 and Table S12). The correlation of M2:M1 TAM ratio and the extent of tumor lymphatic infiltration was also calculated ($r=1.415$, $P=0.001$, linear regression; Figure 5Eiv-2 and Table S13). All these results confirmed that the count of M2 TAMs increased in cervical cancer accompanied by a higher ratio of tumor lymphatic infiltration. In order to explore the expression of high-risk genes that promote cervical cancer lymphatic infiltration, we performed Western blot analysis on cervical cancer LVI-positive and -negative groups (Figure 5Fi). As expected, protein

expression of MMP2, SPARC, and GNLY in the positive group was obviously higher than the negative group. The more M2 TAMs in tumor tissue, the higher the protein expression of MMP2, SPARC, and GNLY.

Accordingly, the OS and RFS of patients were obviously higher in the lower-MMP2-expression group than the higher-MMP2-expression group. OS was 39.2±6.9 vs. 65.3±5.5 months in the latter vs. the former (P<0.05, unpaired t test). RFS was 34.8±7.6 vs. 53.7±6.4 months in the latter vs. the former (Figure 5Fii-1 and Table S14; Figure 5Fii-2 and Table S15), There was a significant difference between the two groups (P<0.05, unpaired t test). The protein expression of MMP2, GNLY, and SPARC was positively correlated with M2 TAMs, indicating that they may damage basal member of tumor lymphatic vessels and increase tumor cells metastasis. As such, from multiple perspectives, increased M2 TAM polarization and related protein activity promoted cervical cancer LVI and reduced the OS of patients.

Single-Cell Data Analysis Confirmed M2 TAM–Polarized Microenvironment Accelerated Cervical Cancer LVI

Cell-Quality Screening and Cell-Type Determination

We screened the single-cell data first. Violin plots show correlation between the total RNA count and the number of mitochondrial RNA or genes (Figure 6Ai-1). Cells with >2500 genes were filtered out, while most of the cell samples possessed less than 30,000 RNAs (Figure 6Ai-2). Most cell samples contained mitochondrial RNA of <15% (Figure 6Ai-3). Therefore, filtering criteria were single cells with <2500 genes and mitochondrial RNA of <15%.

The proportion of mitochondrial RNAs was negatively correlated with the number of total RNAs. The fewer the RNAs, the greater the proportion of mitochondrial RNAs. This indicated that the cell samples may have been damaged (Figure 6Aii-1). The number of genes was positively correlated with the number of total RNAs (Figure 6Aii-2). Volcano plots present gene-expression differences among the top 1500 genes per cell sample. We first screened the single-cell data, selected the top 1500 genes, then gradually obtained the top 10 genes (Figure 6Aiii). These included MMP2, SPARC, and GNLY and were correlated with M2 TAMs accelerating cervical cancer LVI.

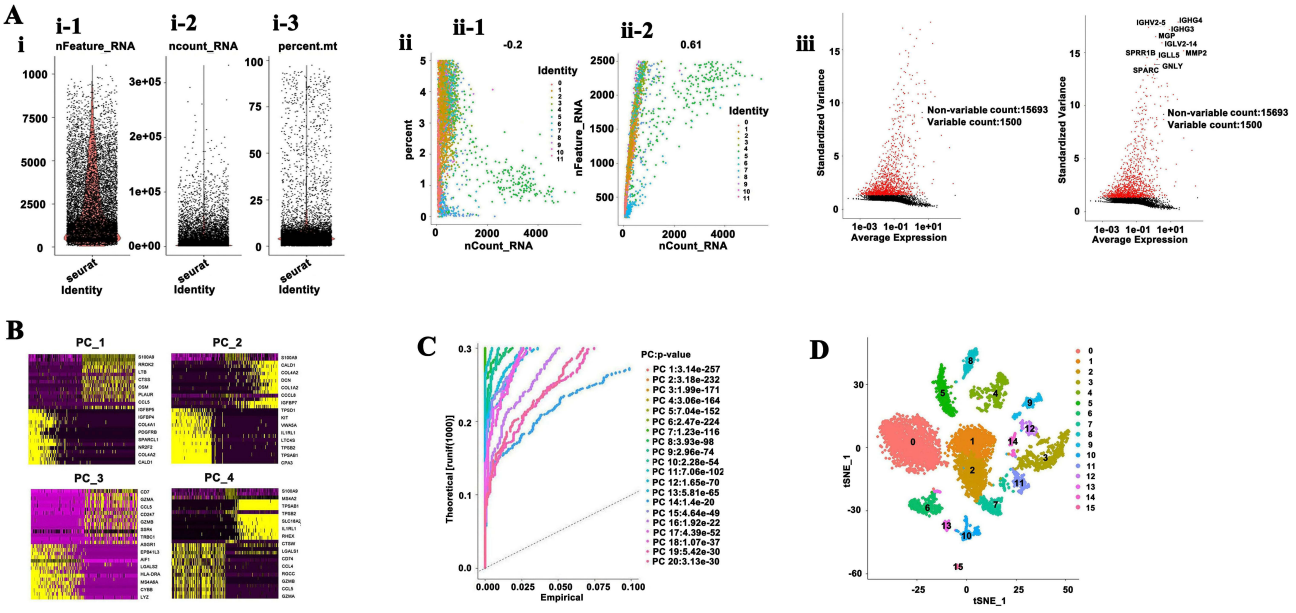

Figure 6 Cell-quality screening and cell-type determination. (**A**) Violin plots of correlation between the total count of RNAs and the number of mitochondrial RNAs. (**Ai-1**) Cells with <2500 genes were filtered out. (**Ai-2**) Most cell samples possessed <30,000 RNAs. (**Ai-3**) Most cell samples contained mitochondrial RNA ratio of <15%. (**Aii-1**) CombinePlots showing the proportion of mitochondrial RNAs was negatively correlated with the number of total RNAs. (**Aii-2**) The number of genes was positively correlated with the number of total RNAs. (**Aiii**) Volcano plots of gene-expression differences among the top 1500 genes per cell sample. (**B**) The DimHeatmap of distribution of the top 15 genes in the first four principal components. (**C**) JackStraw plot of distribution ratio of RNAs for each principal component. (**D**) T-SNE plots dividing data samples into 15 clusters.

The DimHeatmap shows the distribution of the top 15 genes in the first four principal components (PCs) (Figure 6B). Cell types were determined by the reduced dimension function. The JackStraw plot shows the distribution ratio of RNAs (or genes) for each principal component (Figure 6C). T-SNE plots divide the data samples into 15 clusters (Figure 6D).

Pseudotrajectory Construction

Next, we performed pseudotrajectory analysis. T-SNE plots divided TAMs into mainly M1, M2, and other subtype clusters (Figure 7A). TAM markers and related genes *CD14*, *CCL5*, *MMP2*, *SPARC*, *GNLY*, *FOSL2*, *MAF*, and *CTLA4* expressed higher levels in cell clusters according to t-SNE analysis (Figure 7B). Analyzed by BEAM function, a branched heatmap shows the differential genes expression accompanied by pseudotime changes. Columns represent pseudotime, whereas rows represent genes (Figure 7Ci and Table S18). A dendrogram presents the trajectory of main cell clusters in cervical cancer (Figure 7Cii). Pseudotime trajectory analysis exhibited TAM clusters in a two-dimensional state. The M2 TAM-related genes *MMP2*, *SPARC*,

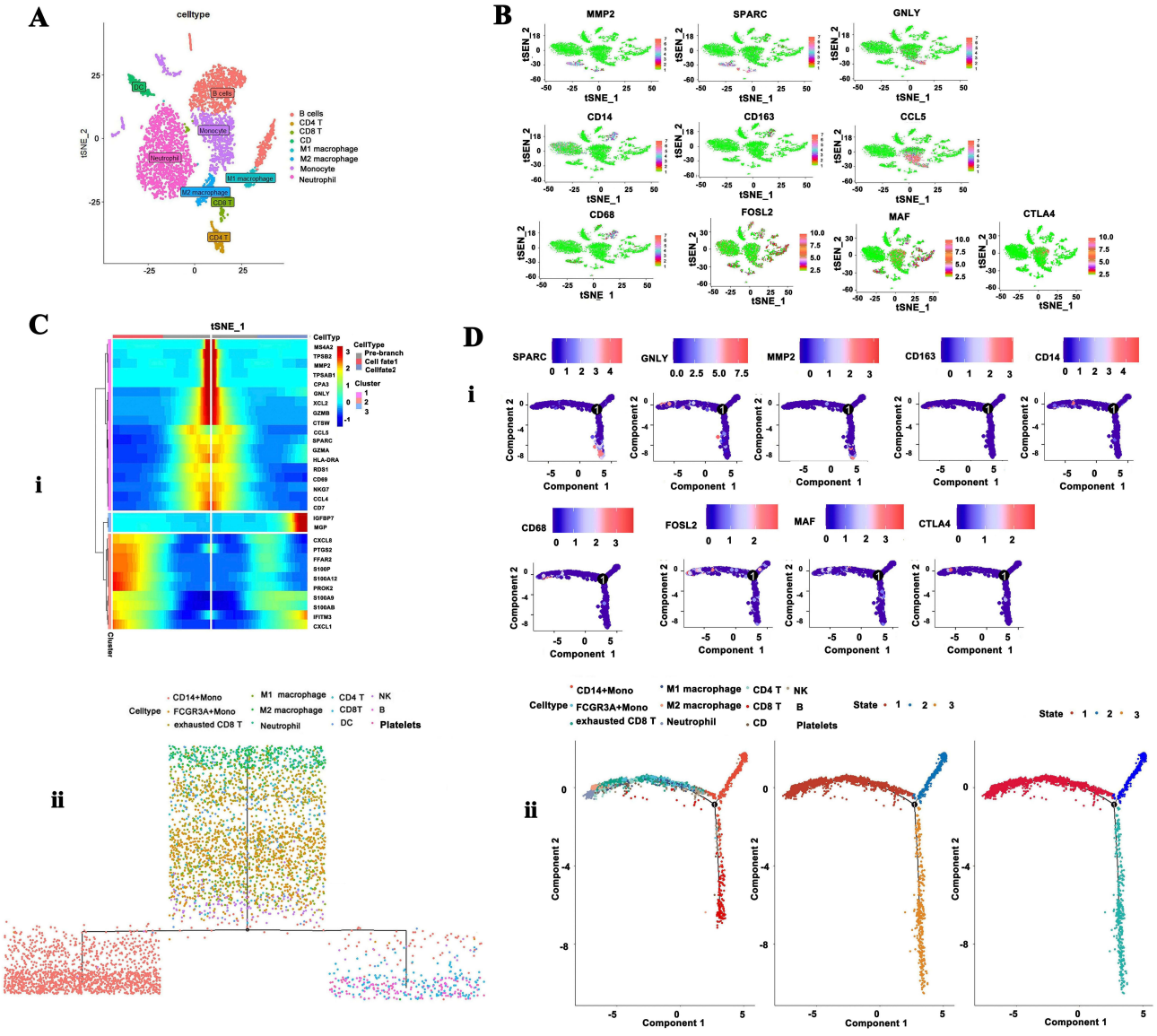

Figure 7 Pseudotrajectory construction. (**A**) T-SNE plots of tumor-associated macrophages (TAMs) and other cell subtypes. (**B**) Scatterplots of M2 TAM markers and the related genes *CD14*, *CCL5*, *MMP2*, *SPARC*, *GNLY*, *FOSL2*, *MAF*, and *CTLA4* that expressed higher levels in cell clusters. (**Ci**) Analyzed by BEAM function, branched heatmap of differential gene expression accompanied by pseudotime changes. (**Cii**) Dendrogram of the trajectory of main cell clusters in cervical cancer. (**Di**) Pseudotime trajectory analysis of TAM clusters in two-dimensional state. The TAM-related genes *MMP2*, *SPARC*, *GNLY*, *FOSL2*, *MAF*, and *CTLA4* expressed higher levels among cell clusters. (**Dii**) Pseudotime trajectory of the main cell subtypes and state.

https://doi.org/10.2147/OTT.S468484 DovePress

GNLY, *FOSL2*, *MAF*, and *CTLA4* expressed higher levels among cell clusters (Figure 7Di). Pseudotime trajectory described the main cell subtypes and state (Figure 7Dii).

DEGs and GSEA

Finally, we carried out gene set enrichment analysis (GSEA) for differentially expressed genes (DEGs). There was a higher density of M2 TAMs (0.65) than M1 TAMs (0.35), suggesting an immunosuppressive environment in cervical cancer (Figure 8Ai). Analyzed by the AddModuleScore function, MMP2, SPARC, and GNLY expressed obviously higher inflammatory levels in M2 clusters than M1 clusters. The M1 (CD68):M2 (CCL5) TAMs ratio decreased significantly (Figure 8Aii).

Similarly, anti-inflammatory, immunosurveillance, and anti–immune escape scores of M1 TAMs were obviously higher than those of M2 TAMs ($P<0.05$), so M2 TAMs played a key role in cervical cancer LVI. M1 TAMs in precancerous lesions presented higher anticancer and proinflammatory scores than in tumors. M2 clusters showed lower immunosurveillance and higher escape scores than M1 and made cancer cells more prone to LVI (Figure 8Aiii). The histogram presents gene-expression rankings for each cell. The quantiles and number of genes were detected in each cell. Total cells and genes were 4879 and 7193, respectively. Quantiles and number of genes (minimum 201) were 1% (243), 5% (310), 10% (339), 50% (339), and 100% (2499) respectively (Figure 8Aiv).

Differentially expressed genes (DEGs) were enriched with GO and KEGG, and are exhibited as heatmaps (Figure 8Bi, Genes, Table S19). The heatmap of genes shows that the expression levels of some genes, such as *MMP2*, *SPARC*, and *GNLY*, were significantly higher in M2 TAM clusters than in M1 clusters. GO analysis showed that innate immunoresponse, monocyte chemotaxis, and cell response to stimuli in M2 TAMs were obviously lower than in M1 TAMs (Figure 8Bi, GO, Table S20). KEGG analysis showed normal cervical tissue and HSIL cluster containing more M1 TAMs, presenting positive regulation of stimuli, chemotaxis, and the immune system process–signaling pathway, whereas cervical cancer and metastatic lymph nodes enriched with M2 TAMs presented negative regulation of these signaling pathways (Figure 8Bi, KEGG, Table S21).

The sketch map illustrates that M2 TAM activity increased gradually from precancerous lesions to cervical cancer. The M2 TAM–related gene *MMP2* destroyed the tumor vasculature basement membrane, and SPARC antiadhesion played a key role in epithelial–mesenchymal transition (EMT) and tumor invasion. M2 TAMs activated cytotoxic T cells

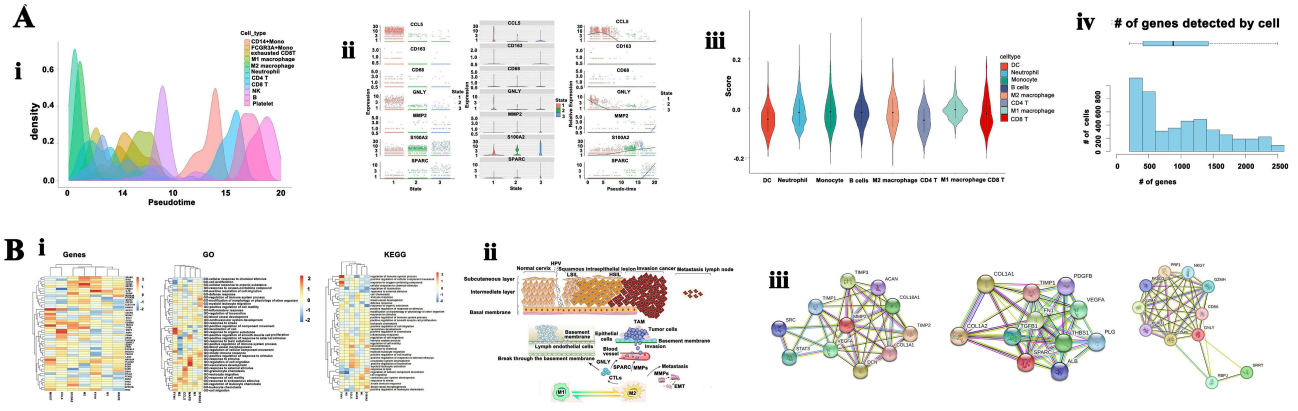

Figure 8 Differentially expressed genes (DEGs) and gene set enrichment analysis (GSEA). (**Ai**) Cell-density plot showing higher density of M2 clusters (0.65) than M1 clusters (0.35). (**Aii**) Scatter- and violin plots showing that MMP2, SPARC, and GNLY expressed significantly higher levels in M2 clusters than in M1. M1 (CD68)/M2 (CCL5) clusters ratio decreased significantly. (**Aiii**) Violin plots showing M2 clusters possessed lower immunosurveillance and higher escape scores than M1. (**Aiv**) Histogram of gene-expression rankings for each cell. #Quantile and the number of genes were detected in each cell. Total number of cells and genes were 4879 and 7193, respectively. Quantile and number of genes (minimum were min(201) were 1% (243), 5% (310), 10% (339), 50% (339), and 100% (2499), respectively. (**B**) (**Bi, Genes**) Differentially expressed genes exhibited with heatmap. (**Bi,GO**) GO analysis were exhibited with heatmap. (**Bi,KEGG**) KEGG analysis exhibited with heatmap. (**Bii**) Sketch map showing M2 TAM activity increased gradually from precancerous lesions to cervical cancer. The M2 TAM–related gene *MMP2* destroyed the tumor vasculature basement membrane, and SPARC antiadhesion played a key role in epithelial–mesenchymal transition and tumor invasion. M2 TAMs activated cytotoxic T cells to release GNLY, which induced the apoptosis of target cells through the formation of pores on the target-cell membrane and assisted tumor lymphovascular infiltration. (**Biii**) Adjacent gene relationships of *MMP2*, *SPARC*, and *GNLY* analyzed with the protein–protein interaction (PPI) function at https://string-db.org/.

to release GNLY, which induced the apoptosis of target cells through the formation of pores on the target-cell membrane and assisted tumor LVI (Figure 8Bii). The adjacent gene relationships of *MMP2*, *SPARC*, and *GNLY* were analyzed with protein–protein interaction networks at https://string-db.org/ (Figure 8Biii).

Potential limitations of the single-cell analysis were dropout events and batch effects. The data were normalized with the "scale data" function in the Seurat package first. We excluded dropout events with the M3DropCleanData and M3DropFeatureSelection functions in M3Drop package during data analysis. We excluded batch effects with the ComBat function in the SVA package or BatchEffect function in the limma package during data analysis. To sum up, through single-cell analysis, we illustrated that M2 TAMs and related genes decreased tumor immunosurveillance and anti–immune escape scores, resulting in an immunosuppressive microenvironment. This microenvironment accelerated cervical cancer LVI.

Discussion

Reports on laparoscopic surgery decreasing the rate of disease-free survival and OS for cervical cancer patients induced researchers to explore other methods, such as increased tumor LVI diagnosis rate for precision surgery, improvement of patient immunity to tumors, analysis of tumor immunoinfiltrating lymphocytes, and application of HPV vaccination and immunocheckpoint inhibitors.[8] Accurate diagnosis of tumor LVI status may guide exact surgical operation scope and improve cervical cancer patients' outcomes. Micrometastases reduce cervical cancer patients' OS and are not easily discovered by routine H&E staining. Ultrastaging and double IHC staining can enhance the diagnostic ratio. It has been found that M2 TAMs increase both inside and outside tumor vasculature in pathological sections. Accumulated evidence indicates that M2 TAMs promote vasculature invasion of cervical cancer. In this study, we carried out CNP mapping combined with ultrastaging and double IHC staining for the detection of cervical cancer LVI. Next, we evaluated the role of TAMs within the tumor microenvironment with flow cytometry, Western blot, and single-cell data analysis.

CNP Mapping as an SLN Screening Tracer in Cervical Cancer

Among the 98 patients in our study, 96 had more than one SLN on CNP mapping. The sensitivity of SLN detection was 98% (96/98), and the accuracy rate was 96.1% (94/98); therefore, CNPs can be deemed a qualified tracing system for SLNs in early-stage cervical cancer to preliminarily detect LVI. Bogani et al[9] reported that sentinel-node mapping was not inferior to conventional lymphadenectomy in identifying patients with endometrial cancer in stage IIIC. SLN mapping combined with ultrastaging can find micrometastases and isolated tumor cells that are not always detectable via conventional pathological detection. Wang et al[10] reported on CNPs being used to detect SLN cervical cancer operation. Only single-antibody IHC was used, with a lower detection rate than our double IHC staining. As such, ultrastaging and double IHC staining may be key factors in ensuring higher identification rates of SLN mapping.

Double IHC Staining Enhanced the Detection Rate of Vasculature Micrometastases in Cervical Cancer

Tumor LVI is related to histological grade associated with worse prognosis, probably reflecting the potential for vasculature spread and aggressive behavior. Tumor micrometastases induce early recurrence and reduce the OS of patients according to our study and previous reports.[11] Lymphatic metastasis is the main route for early cervical cancer development. LVI is an independent predictor of poor prognosis in patients with cervical cancer. Lymphatic vessels are diagnosed based on the presence of tumor emboli within vascular channels lined by a single layer of endothelial cells without red blood cells. Lymphatic vessels are flattened channels or open spaces lined by a single layer of endothelial cells, and the lumina are sometimes filled with lymphocytes. However, the identification of LVI is difficult in H&E-stained slides. Retraction artifacts that isolate tumor aggregates due to tissue shrinkage during fixation are sometimes confused with true tumor emboli in lymphatic vessels. Therefore, H&E staining has a low detection rate and poor repeatability for the assessment of tumor vascular invasion.[12,13]

In this study, H&E and ultrastaging combined with double IHC staining were used, and the detection rate of cervical cancer vasculature micrometastases was significantly higher than that of H&E staining alone. Therefore, D2-40/CD31-CKpan double IHC staining is a reliable method for determining vascular micrometastases. Moreover, our study found

that there was a negative correlation with the OS of patients ($P<0.05$) when the number of vascular invasion foci was greater than two or the number of cancer emboli cells was greater than 5.3. Previous reports have adopted methods of CNP mapping, H&E staining, and monoclonal antibody IHC staining, and some tumor vascular metastases could not be found or misdiagnosed. We integrated methods of CNP mapping, ultrastaging, and double IHC staining, and these methods enhanced the detection of tumor LVI over previously reported methods.

M2 TAMs Enhanced Tumor Lymphatic Vessel Infiltration in Cervical Cancer

Higher numbers of circulating monocytes in patients with cervical cancer indicate poor prognosis, and circulating monocytes are recruited by cervical cancer tissue and differentiate into M1 and M2 TAMs in the tumor microenvironment.[14,15] M1 and M2 cells lose balance in cervical cancer. M1 and M2 are two subtypes of TAMs. M1 TAMs can enhance inflammation and anticancer immunity, and so can inhibit tumor growth. In contrast, M2 TAMs can inhibit inflammation and anticancer immunity and thus promote tumor growth. M2 TAM activity increases gradually from precancerous lesions to cervical cancer. In this study, the ratio of M1:M2 TAMs was 0.58, confirming the tumor microenvironment was polarized toward M2 cell clusters.[16,17]

Based on our double IHC staining, there were obviously more M2 TAMs count surrounding the tumor margin in the group with LVI than in the group without LVI, while the number of M1 TAMs within lymphatic vessels was obviously lower than that in the surrounding tissue. This further proved that the tumor microenvironment was polarized toward M2 cell subtypes. Both our IHC staining and flow cytometry showed higher M2:M1 TAM ratios ($P<0.05$). The number of M2 TAMs was positively correlated with the degree of tumor LVI ($P=0.0024$), indicating that there is an increase in M2 TAMs in tumor LVI infiltration. According to our Western blot analysis, protein expression of MMP2, SPARC, and GNLY in cervical cancer LVI positive group was obviously higher than that of the negative group. Accordingly, the OS and RFS of patients markedly decreased.

Based on our IHC staining and Western blot analysis, the M2 TAM–related proteins MMP2, SPARC, and GNLY expressed higher levels than M1 TAMs in cervical cancer. The M1:M2 ratio decreased significantly. Consistently with previous reports, MMP2 and GNLY were able to destroy the tumor vasculature basement membrane, and SPARC anti-adhesion played a key role in tumor EMT and LVI.[18,19]

In brief, we adopted a method of double IHC staining that visualized tumor LVI and also characterized M2 TAM polarization inside and outside the tumor vasculature at the same time. We integrated an automatic blood cell analyzer, flow cytometry, and Western blot analysis. From multiple perspectives, we explored the mechanism of M2 TAM polarization and related gene activity, accelerated cervical cancer LVI, and reduced patient OS.

Cervical Cancer Single-Cell Data Collection and Analysis

In this study, single-cell data on cervical cancer were obtained, screened, and reduced in dimension and pseudotrajectories were constructed. Differentially expressed gene (DEG) analysis showed that the expression of the M2 cluster–related genes *MMP2*, *SPARC*, and *GNLY* was significantly higher than that of M1 clusters in cervical cancer, and the M1:M2 cluster ratio decreased significantly. MMP2 and GNLY can destroy the basement membrane of the tumor vasculature, and SPARC antiadhesion plays a key role in tumor EMT and LVI, as mentioned above.

Based on the calculated inflammatory scores, M1 clusters' anti-inflammatory, immunosurveillance, and anti–immune escape scores were higher than those of M2 clusters, indicating that M2 clusters play a key role in cervical cancer LVI. M1 clusters in precancerous lesions had higher anticancer and proinflammatory scores than those in tumors. M2 clusters showed lower immunosurveillance and higher escape scores than other cell clusters, endowing cancer cells with a stronger ability to invade the tumor vasculature. GO analysis showed that innate immunoresponse gene expression of M2 clusters was obviously lower than that of M1 clusters and that the normal cervical tissue and HSIL cluster had higher enrichment of M1 clusters, presenting positive regulation of the response stimulus signaling pathway, whereas cervical cancer and metastatic lymph nodes enriched M2 clusters, presenting negative regulation of these signaling pathways.

Single-cell data analysis indicated that M2 TAM activity gradually increased from the precancerous lesions to cervical cancer. HSIL showed a less active tumor microenvironment, and the main components included $CD8^+$ T cells, Tregs, DC1, and M1 TAMs. DC1 effectively activated the key effects of CTL antitumor immunity. Tregs can

inhibit T-cell and M1 TAM activation. The balance between these two factors determines tumor growth. The tumor tissue presented an immunosuppressive environment and the main components included exhausted $CD8^+$ T cells and M2 TAMs. The exhausted $CD8^+$ T cells lost their immunosuppressive function. M2 TAMs inhibited cytotoxic $CD8^+$ T-cell anticancer immunity and promoted tumor vasculature invasion.

Metastatic lymph nodes showed an early phase of immunoreaction, including naïve $CD4^+$ T cells, effector memory $CD8^+$ T cells, cytotoxic $CD8^+$ T cells, and TAM markers by S100A8. In addition to the aforementioned mechanism, TAMs inhibited cytotoxic $CD8^+$ T cells by increasing Treg cell numbers. Tregs and Th17 cells are subtypes of $CD4^+$ T cells. Tregs can inhibit T cells, while Th17 cells can activate cytotoxic $CD8^+$ T cells. The number of Tregs released by TAMs was significantly higher than that released by Th17 cells. Therefore, Tregs inhibit cytotoxic $CD8^+$ T cell activation and promote tumor growth.[18]

Different methods could be used to enhance patients' antitumor immunoabilities in different stages of cervical cancer. IL, IFN, and DC vaccines can be used to treat precancerous lesions in cervical cancer treatment.[19] TAMs reached 30%–50% of stromal cells. As that study showed, M2 TAMs inhibited antitumor immunity and enhanced tumor vasculature invasion. Therefore, TAMs are an important therapeutic target, and the production of functional nanomedicines by TAMs or reprogramming TAMs have both been envisioned as new methods for tumor immuno-oncology that may be able to achieve satisfactory clinical results.[19,20] In short, we analyzed cervical cancer LVI mechanisms with single-cell data. We further illustrated M2 TAMs and related genes decreased tumor immunosurveillance and anti–immune escape scores, resulting in an immunosuppressive microenvironment. This microenvironment accelerated cervical cancer LVI.

M2 TAM–Related Genes as Novel Candidate Biomarkers in Immunotherapy

Immunocheckpoint-inhibitor therapy has revolutionized treatment for advanced tumors, but a limited population benefits from this treatment. Thus, screening novel biomarkers is urgently needed to address this concern.[21] Based on our single-cell data, both scatterplot and pseudotime trajectory analyses revealed higher expression of the M2 cluster–related genes *MMP2*, *SPARC*, *GNLY*, *FOSL2*, *MAF*, and *CTLA4*.

TAMs promote tumor growth and immunosuppression, but how TAMs develop from circulating monocytes and local tissue–resident macrophages remains incompletely understood. Using a model of pancreatic ductal adenocarcinoma in monocyte fate–mapping mice, Dunsmore et al examined the dynamics of the monocyte-to-macrophage transition in tumors. FOSL2 may play a role in the transition of monocytes to TAMs. MAF is a transcription factor that plays a key role in regulating the differentiation of TAM2 populations, and is a potential target for cancer immunotherapy.[22]

CTLA4 is an essential immunomolecule that plays a vital role in cell-cycle modulation, regulation of T-cell proliferation, and cytokine production. Inhibition of overexpression of immunocheckpoints, such as CTLA4 receptors, has been confirmed as an effective strategy in cancer therapy.[23] Our study found higher expression of the M2 cluster–related genes *MMP2*, *SPARC*, *GNLY*, *FOSL2*, *MAF*, and *CTLA4*. The high-risk genes *MMP2*, *SPARC*, and *GNLY* promoted LVI in cervical cancer, while *FOSL2*, *MAF*, and *CTLA4* played a key role in M2 TAM transition. These genes maybe be novel candidate biomarkers for immunocheckpoint-inhibitor therapy.

Strengths and Limitations of This Study

This study focused on the detection of LVI in cervical cancer and the mechanism of TAMs promoting vasculature metastasis. We integrated CNP mapping, IHC staining, flow cytometry, Western blotting, and single-cell sequence bioinformation analysis. These methods not only improved the detection ratio of vasculature micrometastasis for cervical cancer but also deepened our understanding of the mechanisms of TAMs in vasculature micrometastasis.

We note that although there have been previous reports on one of the aforementioned factors, there is still little comprehensive research on LVI in cervical cancer from clinical practice to theoretical basis like ours. Xinyu et al reported[24] on the use of intraoperative pelvic lymph-node frozen pathology to predict patient prognosis, while H&E staining is still not very exact in comparison to double IHC double staining.

Strengths

The integration of CNP mapping, ultrastaging, and double IHC staining enhanced the determination of cervical cancer LVI over previous reports. The mechanisms were explored from multiple perspectives, i.e. polarization of M2 TAMs, increase in related genes activity accelerating tumor LVI, and reduced patient OS. All of the flow cytometry, Western blotting, and cervical single-cell data showed thyat M2 cluster–related genes expressed higher levels. These genes perhaps could be used as novel candidate biomarkers in immunocheckpoint-inhibitor therapy.

Limitations

Only intraoperative freezing and H&E staining incorporated CNP mapping, while IHC staining could not be carried out to form guidance for lymph-node dissection immediately. Only GEO single-cell data were used for direct cervical cancer sample examination.

To sum up, accurate determination of LVI status may guide exact surgical operation scope and improve cervical cancer patient outcomes. CNP mapping could be used for SLN tracing in early cervical cancer LVI. Double IHC staining could enhance diagnostic efficiency over H&E staining in determining LVI. M2 TAM activity increased, forming an immunosuppressive environment in cervical cancer tissue, and M2 TAM–related genes could play a key role in this process and be used as novel candidate biomarkers in immunotherapy. TAMs are becoming a research hotspot in tumor immunotarget therapy.

The significance of this study lies in elucidating the interaction between TAMs and cervical cancer cells, as well as how this interaction influences tumor LVI and patient survival. This research exhibited enhanced detection of microvascular metastasis in cervical cancer through various methodologies, including CNP mapping, H&E staining, and double IHC staining. The findings revealed a positive correlation between the number of M2 TAMs and the extent of LVI in cervical cancer. Furthermore, an increased ratio of M2 to M1 TAMs was associated with a higher incidence of tumor LVI. Additionally, the study investigated the expression levels of high-risk genes, such as *MMP2*, *SPARC*, *GNLY*, that promote LVI in cervical cancer, while *FOSL2*, *MAF*, and *CTLA4* play key roles in M2 TAM transition. These genes could be used as novel candidate biomarkers in immunocheckpoint-inhibitor therapy. These results contribute to a deeper understanding of the role played by TAMs within the cervical cancer microenvironment and offer potential targets for personalized therapeutic strategies.

The mechanisms of TAM action imply that the potential for personalized treatment strategies can be based on TAM density in clinical practice. We recommend future studies evaluate the efficacy of combining TAM-targeted therapies with immunocheckpoint inhibitors. This could also be expanded to include specific types of preclinical models or clinical trial designs that would be most informative.

Data Sharing

We have made provisions for all materials described in our manuscript, including all relevant raw data, to be freely available to any researchers who may wish to reuse or reanalyze them. The datasets contained in Figures 6, 7 and 8 and Tables S16–S21, were downloaded from https://www.ncbi.nlm.nih.gov/gds/?term=GSM6360680. This paper has been uploaded as a preprint: https://www.researchgate.net/publication/379284375;https://www.researchsquare.com/article/rs-4022648/v1.

Ethics Approval and Consent to Participate

This study was approved by the ethics committee of our hospital (ZBLL2022102402001) and designed in line with the Declaration of Helsinki in terms of human rights. In this study, resected cervical cancer samples were used for pathological detection and blood samples were used for monocyte detection. The patients were informed of the risks and benefits of participating in the study and signed written agreements.

Patient Consent for Publication

The patients provided informed consent for the publication of the detected results and signed a written agreement. No personal privacy information was involved, and these studies did not cause additional harm to patients.

Acknowledgments

We thank Mrs. Cuihua Zhang from the Department of Pathology, Chifeng Cancer Hospital, Inner Mongolia, China for providing technical support for IHC pathology. We thank Mr. Erqiang Hu from Southern Medical University, Guangzhou, China, for his help with the R code bioinformatic analysis.

Author Contributions

All authors made a significant contribution to the work reported, whether in the conception, study design, execution, acquisition of data, analysis, and interpretation, or all these areas, took part in drafting, revising, or critically reviewing the article, gave final approval to the version to be published, have agreed on the journal to which the article has been submitted, and agree to be accountable for all aspects of the work.

Funding

This study was supported by the Jing'an District Science and Medical Technology Project (2022MS07).

Disclosure

The authors declare they have no conflicts of interest in this work.

References

1. Sung H, Ferlay J, Siegel RL, et al. Global cancer statistics 2020: GLOBOCAN estimates of incidence and mortality worldwide for 36 cancers in 185 countries. *CA Cancer J Clin*. 2021;71(3):209–249. doi:10.3322/caac.21660
2. NCCN Guidelines. *National Comprehensive Cancer Network. NCCN Clinical Practice Guidelines in Oncology (NCCN Guidelines) Cervical Cancer Version 1*. Plymouth Meeting, PA: National Comprehensive Cancer Network; 2021.
3. Ramirez PT, Frumovitz M, Pareja R, López A, Vieira M, Ribeiro, R. Phase III randomized trial of laparoscopic or robotic versus abdominal radical hysterectomy in patients with early-stage cervical cancer: LACC Trial. *Gynecol Oncol*. 2018;149:245. doi:10.1016/j.ygyno.2018.04.552
4. Sun W, Chen X, Fu S, et al. Feasibility of sentinel lymph node mapping with carbon nanoparticles in cervical cancer: a Retrospective Study. *Cancer Control*. 2023;30:10732748231195716. doi:10.1177/10732748231195716
5. Bézu C, Coutant C, Ballester M, et al. Ultrastaging of lymph node in uterine cancers. *J Exp Clin Cancer Res*. 2010;29(1):5. doi:10.1186/1756-9966-29-5
6. Kurmyshkina O, Kovchur P, Schegoleva L, et al. Markers of angiogenesis, lymphangiogenesis, and epithelial–mesenchymal transition (Plasticity) in CIN and early invasive carcinoma of the cervix. exploring putative molecular mechanisms involved in early tumor invasion. *Int J Mol Sci*. 2020;21(18):6515.
7. Kabasawa T, Ohe R, Ye Aung N, et al. Potential role of M2 TAMs around lymphatic vessels during lymphatic invasion in papillary thyroid carcinoma. *Sci Rep*. 2021;11(1):1150. doi:10.1038/s41598-020-80694-3
8. Schubert M, Olaf Bauerschlag D, Muallem MZ, et al. Challenges in the diagnosis and individualized treatment of cervical cancer. *Medicina* 2023;59(5):925. doi:10.3390/medicina59050925
9. Bogani G, Giannini A, Vizza E, et al. Sentinel node mapping in endometrial cancer. *J Gynecol Oncol*. 2024;35(1):e29. doi:10.3802/jgo.2024.35.e29
10. Wang Y, Dan Z, Yuan G, et al. Detection of sentinel lymph node in laparoscopic surgery for uterine cervical cancer using carbon nanoparticles. *J Surg Oncol*. 2020;122(5):934–940. doi:10.1002/jso.26100
11. Petrillo M, Zannoni GF, Martinelli E, et al. Polarisation of tumor-associated macrophages toward M2 phenotype correlates with poor response to chemoradiation and reduced survival in patients with locally advanced cervical cancer. *PLoS One*. 2015;10(9):e0136654. doi:10.1371/journal.pone.0136654
12. Zhe G, Ding S. The crosstalk between tumor-associated macrophages (TAMs) and tumor cells and the corresponding targeted therapy. *Front Oncol*. 2020;10:590941. doi:10.3389/fonc.2020.590941
13. Xiong L, Zhang Q, Chen G, Luo D. Multi-Omics analysis showed the clinical value of gene signatures of C1QC+ and SPP1+ TAMs in cervical cancer. *Front Immunol*. 2021;12:694801. doi:10.3389/fimmu.2021.694801
14. Liu X, Guoying N, Zhang P, et al. Single-nucleus RNA sequencing and deep tissue proteomics reveal distinct tumour microenvironment in stage-I and II cervical cancer. *J Exp Clin Cancer Res*. 2023;42(1):28. doi:10.1186/s13046-023-02598-0
15. Pei-Heng L, Kong X-Y, He Y-Z, et al. Recent developments in application of single-cell RNA sequencing in the tumour immune microenvironment and cancer therapy. *Mil Med Res*. 2022;9(1):52. doi:10.1186/s40779-022-00414-y
16. Zhang H, Liu L, Liu J, et al. Roles of tumor-associated macrophages in anti-PD-1/PD-L1 immunotherapy for solid cancers. *Mol Cancer*. 2023;22(1):58.2. doi:10.1186/s12943-023-01725-x
17. Feng Y, Zhiqiang Y, Song F, et al. The role of TAMs in tumor microenvironment and new research Progress. *Stem Cells Int*. 2022;2022:5775696. doi:10.1155/2022/5775696
18. Liu M, Liu L, Song Y, et al. Targeting macrophages: a novel treatment strategy in solid tumors. *J Transl Med*. 2022;20(1):586. doi:10.1186/s12967-022-03813-w
19. Wei X, Wang J, Liang M, et al. Development of functional nanomedicines for tumor associated macrophages-focused cancer immunotherapy. *Theranostics*. 2022;12(18):7821–7852. doi:10.7150/thno.78572

20. Khan S, Khan MU, Muhammad Azhar Ud D, et al. Reprogramming tumor-associated macrophages as a unique approach to target tumor immunotherapy. *Front Immunol*. 2023;14:1166487. doi:10.3389/fimmu.2023.1166487
21. Chen H, Yang W, Zhigang J. Machine learning-based identification of tumor-infiltrating immune cell-associated model with appealing implications in improving prognosis and immunotherapy response in bladder cancer patients. *Zhigang Ji Front Immunol*. 2023;31(14):1171420. doi:10.3389/fimmu.2023.1171420
22. Dunsmore G, Guo W, Li Z, et al. Timing and location dictate monocyte fate and their transition to tumor-associated macrophages. *Sci Immunol*. 2024;9(97):eadk3981. doi:10.1126/sciimmunol.adk3981
23. Babamohamadi M, Mohammadi N, Faryadi E, et al. Anti-CTLA-4 nanobody as a promising approach in cancer immunotherapy. *Cell Death Dis*. 2024;15(1):17. doi:10.1038/s41419-023-06391-x
24. Xinyu Q, Qiu J, Jiang L, et al. Intraoperative frozen pathology exam of common iliac lymph nodes and para-Aortic lymphadenectomy on the prognosis and quality of life for patients with IB2-IIA2 cervical cancer: trial protocol for a randomized controlled trial (C-PACC trial). *J Gynecol Oncol*. 2023;34(2):e13. doi:10.3802/jgo.2023.34.e13